PIC AND FLUID SIMULATIONS OF LOW PRESSURE MAGNETIZED PLASMAS FOR ELECTRIC PROPULSION

Mario Merino, Eduardo Ahedo, Diego García-Lahuerta,
Matteo Guaita, Pedro Jiménez

77th Annual Gaseous Electronics Conference,
San Diego (CA, USA), September 30 – October 4 2024

INTRODUCTION

- This talk is focused on **recent advances on modeling Magnetic Nozzle (MN) physics**
  - Tomorrow 8:30AM, we will talk on **kinetic simulations for Hall Thruster physics**

- The MN is the external, diverging part of the magnetic field in many EPTs (e.g. HPT and ECRT)
  - The $\boldsymbol{B}$ field guides the plasma, limiting its radial expansion contactlessly
  - The magnetic force on the azimuthal plasma currents creates magnetic thrust
  - Thermal energy in the plasma is converted into directed kinetic energy, increasing propulsive efficiency
  - In EPTs, ions are essentially demagnetized downstream and readily separate from the field lines

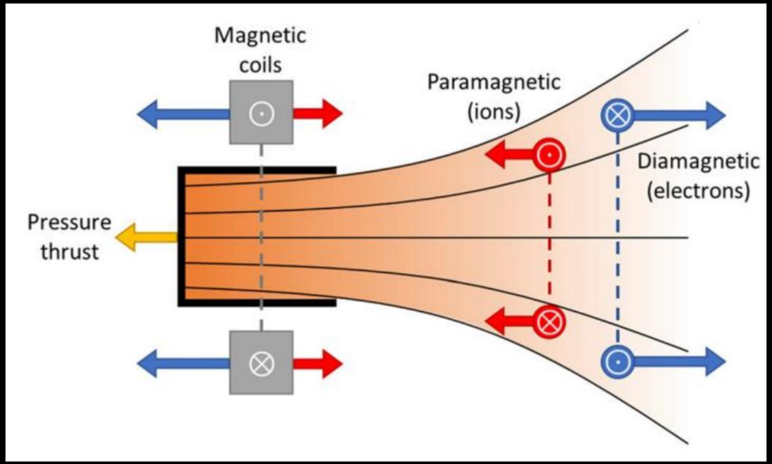

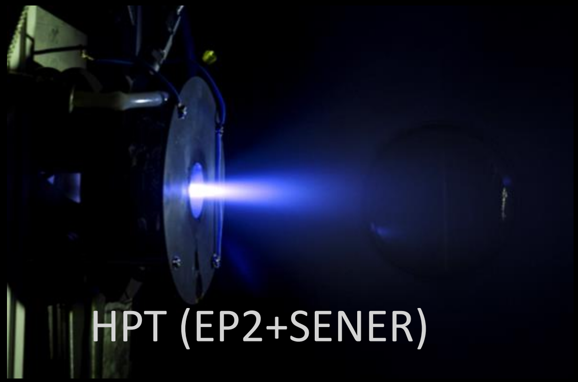

INTRODUCTION

- Ample contributions to MN physics

Fundamentals of 2D MNs for propulsion	POP 2010
MN with double layers	POP 2011
Mechanisms of ion detachment	POP 2011, 2012, 2014
The effects of the induced magnetic field	POP 2016
The effects of hot ions	IEEE 2015
Fully magnetized ions	POP 2016, PSST 2021
Thrust vectoring with 3D MNs	PSST 2017, POP 2018
Collisionless electron cooling (in paraxial MNs)	POP 2015; PSST 2018, 2020, 2021
Applications: MNs in HPT and ECRTs	PSST 2018-2023

- Fluid, Vlasov, PIC based models are selected to analyze different aspects of the problem & levels of detail

- In this talk, we presents recent advances:
  - An electromagnetic implicit full-PIC code to simulate a paraxial MN with RHP waves
  - Fluid and hybrid simulations of a Magnetic Arch (i.e. 2 connected MNs)

References

1. P. Jiménez, L. Chacon and M. Merino (2024): "An implicit, conservative electrostatic particle-in-cell algorithm for paraxial magnetic nozzles", Journal of Computational Physics, 502 112826
2. P. Jiménez, M. Merino, L. Chacón (2024), An Implicit Energy- and Charge- conserving Electromagnetic PIC algorithm for Paraxial Magnetic Nozzles, 38th IEPC, Toulouse, France.
3. M. Merino, D. García-Lahuerta and E. Ahedo (2023): "Plasma acceleration in a magnetic arch", Plasma Sources Science and Technology, 32 065005
4. M. Guaita, M. Merino, E. Ahedo (2024), Hybrid Fluid-PIC Simulations of the Plume Expansion in a Magnetic Arch, 38th IEPC, Toulouse, France.

All our works and extra information at:

https://erc-zarathustra.uc3m.es/

https://ep2.uc3m.es/

PLASMA AND EM WAVES PROPAGATION IN MNs

- Hybrid 2D sim. for ECRT
  Sanchez et al. PSST 2021
- Hybrid 2D sim. for HPT
  Jimenez et al. PSST 2023
- Vlasov sim. of paraxial MN
  Zhou et al. PSST 2021

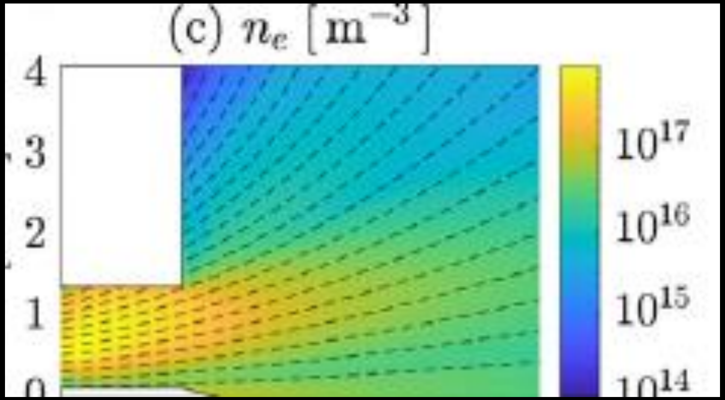

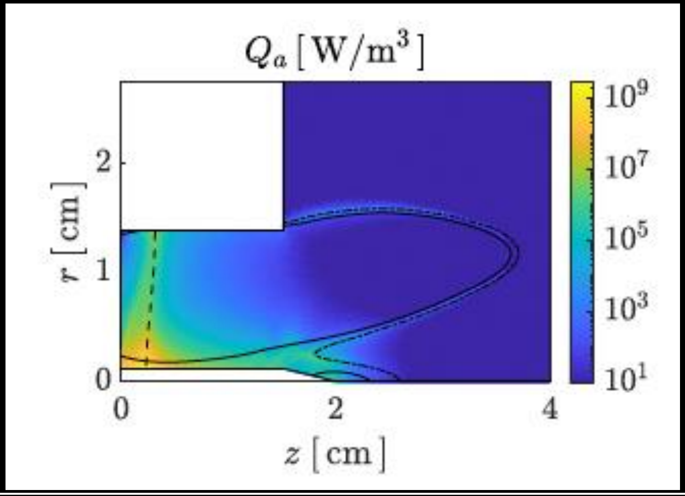

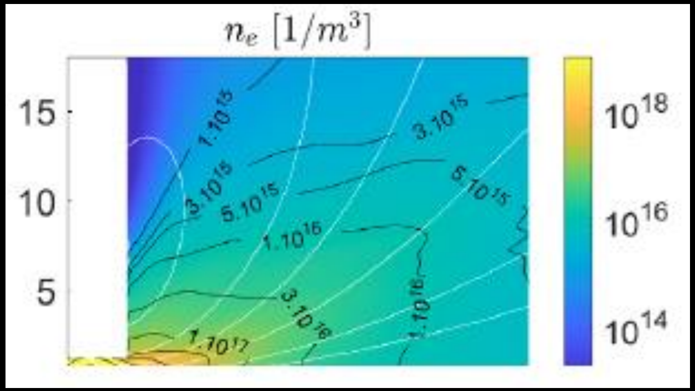

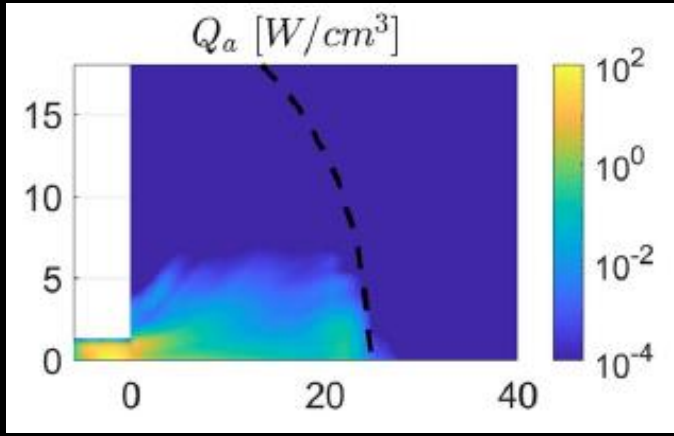

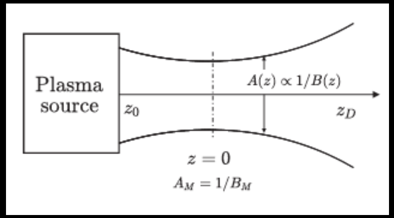

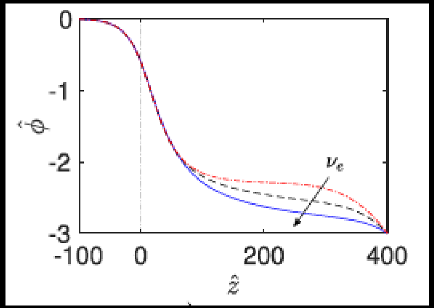

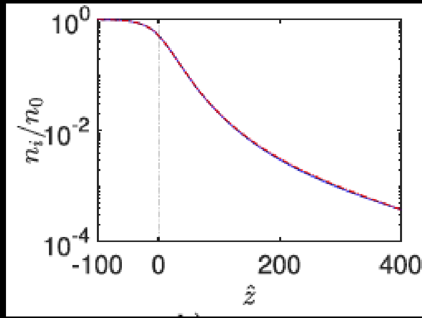

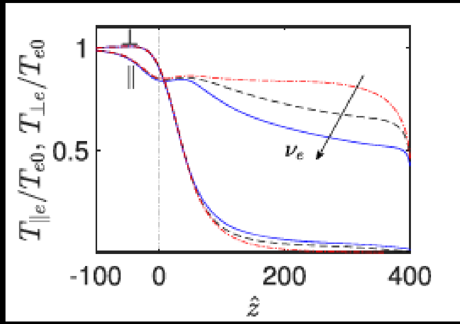

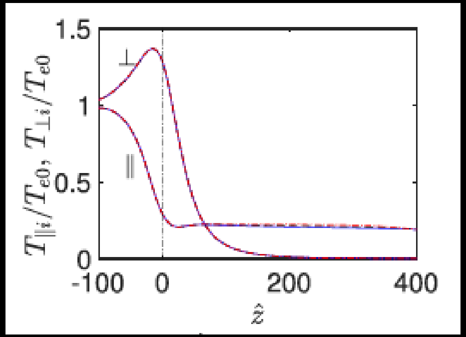

TIME-IMPLICIT PIC ALGORITHM

- Quasi-1D/3V code developed in collaboration with LANL (Luis Chacón)
- Energy conserving, time-implicit scheme overcomes many limitations of explicit PIC codes:
  - $\Delta x > \lambda_{Debye}$ (finite-grid instability) → we can have coarser spatial resolution
  - $\omega_{pe}\Delta t > 1$ (plasma oscillations) → Time step is not limited
  - IPIC can be more efficient for long time and large-scale simulations
- "Particle enslavement" to the ES/EM potentials reduces the size of the nonlinear problem, as residual G can be formulated in terms of Φ^{n+1} only:

$$x_p^{n+1} = x_p[\Phi^{n+1}]; \qquad v_p^{n+1} = v_p[\Phi^{n+1}]$$

$$G\left(x_p^{n+1}, v_p^{n+1}, \Phi^{n+1}\right) = G(x[\Phi^{n+1}], v[\Phi^{n+1}], \Phi^{n+1}) = \tilde{G}(\Phi^{n+1})$$

- Spacetime location of field, current, potential variables important →
- Fully Implicit Crank Nicolson mover
  - **Energy**- and local **charge**- conserving
  - Time centered, 2nd order, non-dissipative
  - Subcycling: Keeps errors in momentum conservation small.
- Jacobian Free Newton Krylov (JFNK) + GMRES
  - Preconditioners can be implemented

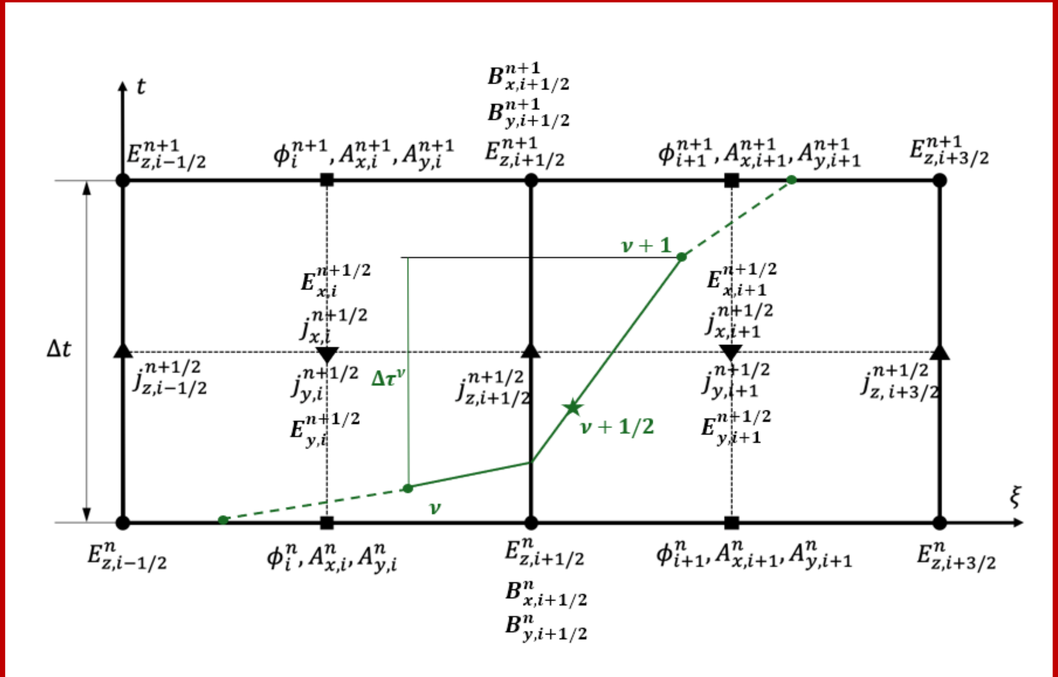

GOVERNING PARTICLE EQUATIONS: MN MODEL

$$\frac{\partial f_s}{\partial t} + \boldsymbol{v}\cdot\nabla_{\boldsymbol{x}} f_s + \frac{q_s}{m_s}\left(\boldsymbol{E} + \boldsymbol{v}\times(\boldsymbol{B}+\boldsymbol{B}_0)\right)\cdot\nabla_{\boldsymbol{v}} f_s = 0,$$

$$f_s(z, v_z, \tilde{\mu}, t) = \sum_{p\in s} w_p \delta(z - z_p(t))\delta(v_z - v_{z,p}(t))\delta(\tilde{\mu} - \tilde{\mu}_p(t))$$

$$v_\parallel \approx v_z \;;\; E_\parallel \approx E_z \;;\; \mathbf{B} \approx B(z)\mathbf{z}\,;\, R\frac{\partial \ln B_{z0}}{\partial z} = \varepsilon \ll 1.$$

- Vlasov equation: collisionless expansion
- Particle discretization of the EVDF
- Paraxial approximation
- Fully magnetized ions

$$\frac{\ell_s}{R} \leq O(\varepsilon),$$

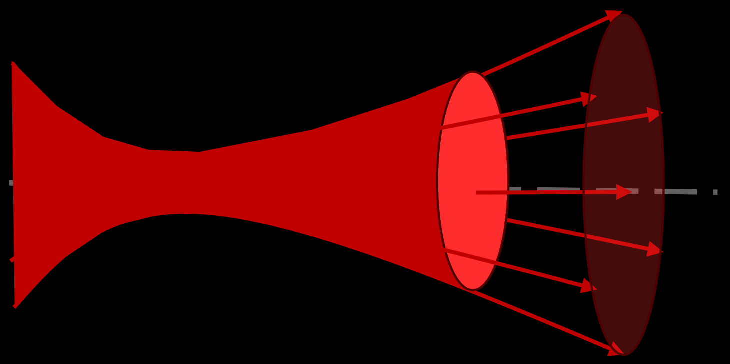

$$\frac{\mathrm{d}z_p}{\mathrm{d}t} = v_{z,p},$$

$$\frac{\mathrm{d}v_{z,p}}{\mathrm{d}t} = \frac{q_s}{m_s}\left(E_z + v_{xp}B_y - v_y B_x\right) - \frac{1}{2B_{z0}}\frac{\partial B_{z0}}{\partial z}\left(v_{xp}^2 + v_{yp}^2\right),$$

$$\frac{\mathrm{d}v_{xp}}{\mathrm{d}t} = \frac{q_s}{m_s}\left(E_x + v_{yp}B_{z0} - v_{zp}B_y\right) + \frac{1}{2B_{z0}}\frac{\partial B_{z0}}{\partial z} v_{zp}v_{xp},$$

$$\frac{\mathrm{d}v_{yp}}{\mathrm{d}t} = \frac{q_s}{m_s}\left(E_y - v_{xp}B_{z0} + v_{zp}B_x\right) + \frac{1}{2B_{z0}}\frac{\partial B_{z0}}{\partial z} v_{zp}v_{yp}.$$

- **ES case**: Applied B_{z0} and ambipolar E_z only.
- **EM case**: Adds wave fields B_x, B_y and E_x, E_y

- Evolution equations for the particles. Q1D-3V system.
  - Magnetic mirror force term.
- 1D-1V if μ is assumed constant (only electrostatic case).

- Scalar and vector potentials (Coulomb's gauge $\nabla \cdot \boldsymbol{A} = 0$) on Maxwell's equations:

$$\boldsymbol{E}_i = -\nabla\phi; \quad \boldsymbol{E}_s = -\frac{\partial \boldsymbol{A}}{\partial t}; \quad \boldsymbol{B}_s = \nabla \times \boldsymbol{A}.$$

$$\nabla \cdot \boldsymbol{E}_i = \frac{\rho}{\varepsilon_0}$$

$$\nabla \times \boldsymbol{B}_s = \mu_0 \varepsilon_0 \frac{\partial \boldsymbol{E}_i + \boldsymbol{E}_s}{\partial t} + \mu_0 \boldsymbol{j}$$

$$-\nabla^2 \phi = \frac{\rho}{\varepsilon_0}.$$

$$-\nabla^2 \boldsymbol{A} = -\mu_0 \varepsilon_0 \left(\frac{\partial \nabla \phi}{\partial t} + \frac{\partial^2 \boldsymbol{A}}{\partial t^2} \right) + \mu_0 \boldsymbol{j};$$

- Terms neglected in Darwin approximation
- Hyperbolic eqs (Maxwell) → Elliptic eqs (Darwin)
- No CFL condition for speed of light (vacuum light waves are removed)
- Darwin is a very good approx. in dense plasmas

Darwin, quasi 1D. →. $A_z = 0$

- Decoupled axial and transverse fields:

$$\epsilon_0 \frac{\partial}{\partial t} \frac{\partial}{\partial z} \left(J^B \frac{\partial \phi}{\partial z} \right) = \frac{\partial (J^B j_z)}{\partial z},$$

$$\left(J^B = \frac{1}{B} \right)$$

$$\frac{\partial}{\partial z} \left(J^B \frac{\partial A_x}{\partial z} \right) = -\mu_0 J^B j_x,$$

$$\frac{\partial}{\partial z} \left(J^B \frac{\partial A_y}{\partial z} \right) = -\mu_0 J^B j_y.$$

ELECTROMAGNETIC SIMULATION SETUP

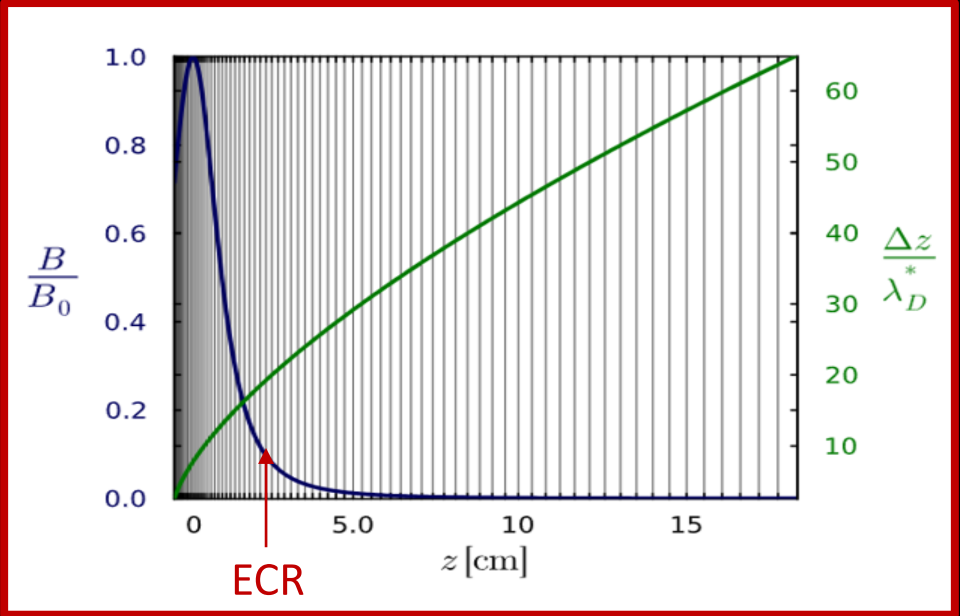

- Plasma conditions close to ECRT or HPT plumes
  - Convergent-divergent nozzle
  - Domain ~ 0.2 m
  - Density $n_e = 10^{18}\ m^{-3}$
  - Electron temperature $T_e = 10\ eV$
  - ECR surface at $z \sim 2.2$ cm.

- Reduced mass-ratio, $m_i/m_e = 100$
  - to lower ion transient time
- $L\omega_{pe}/c$ artificially increased
  - to observe several wave cycles upwards the resonance

- Simulation cases:
  - **ES:** Electrostatic (i.e, no wave).
  - **EM:** Darwin, self-consistent wave simulation. Low and high-power cases.
  - **IW**: wave fields precomputed from cold-plasma dielectric tensor model.

EM Fields and Power Absorption

- Wavefields propagate up to the resonance, where large absorption takes place
- Kinetic results were used to tune damping ratio γ of cold-plasma model
  - γ controls mainly the width of the absorption region.
  - In this case with kinetic damping only: $\gamma \simeq 0.5\omega$ offers a good fit
- Minor differences in phase and magnitude between EM and IW cases.
- Simple fits could be derived over a range of problems of interest

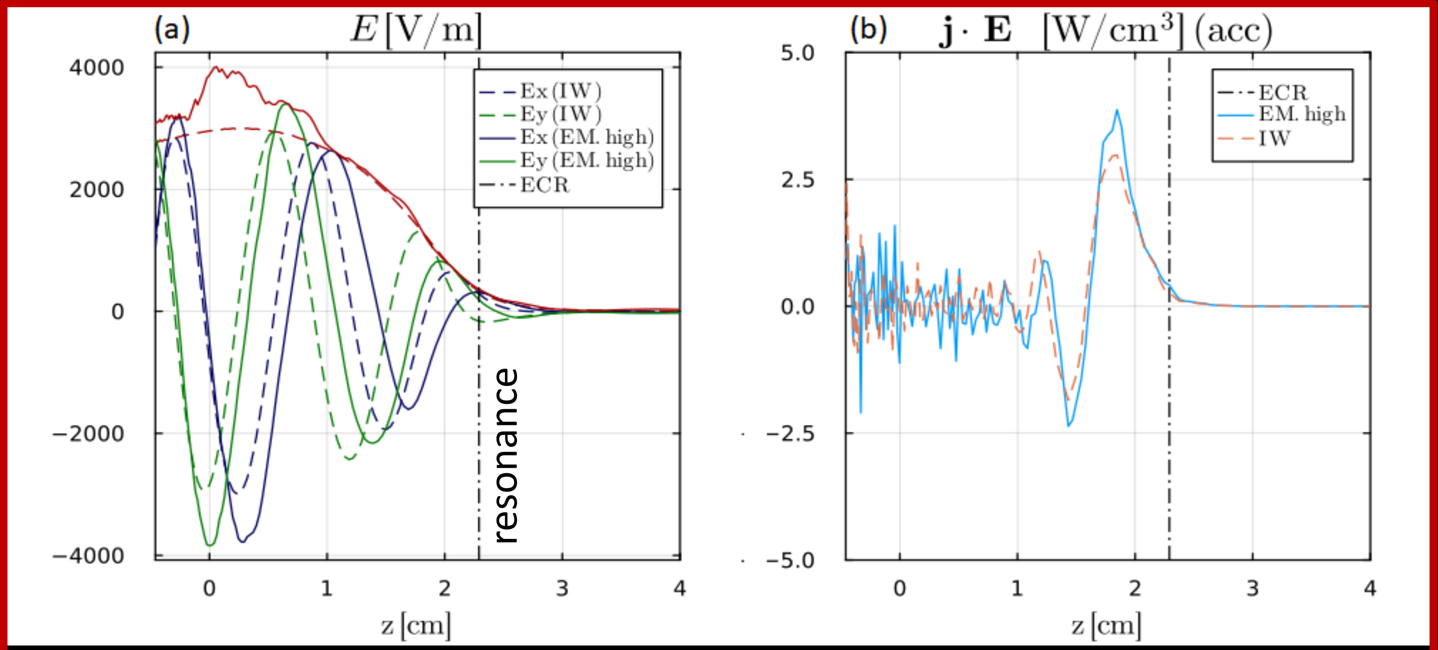

- **ES:** Electrostatic
- **EM:** Darwin, self-consistent wave simulation.
- **IW**: Cold-plasma dielectric tensor model.

Steady state results: Potential and Ion Acceleration

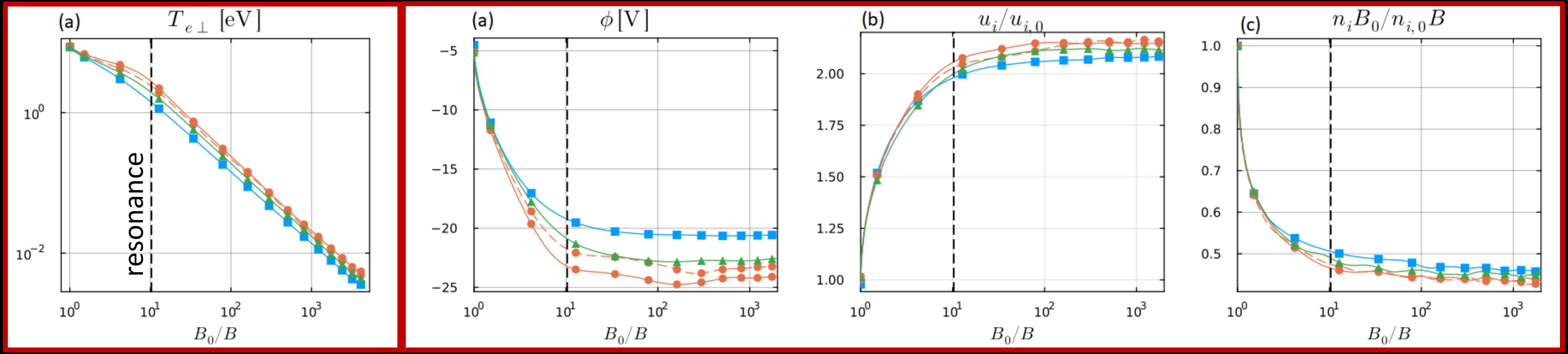

cases ES (■), EM.low (▲), EM.high (● solid) and IW (● dash).

- Larger $T_{\perp e}$ under the presence of RHP wave; increases in the neighborhood of the resonance
- Greater electrostatic potential fall along the MN, consequently greater Ion velocity ($u_i \propto \sqrt{-\phi}$) and larger expansion ($n_i u_i/B = \text{const}$)

ADVANTAGES OF THE IMPLICIT PIC APPROACH

- Time-implicit PIC code → breaks λ_{De} and ω_{pe} constraints. Exact global-energy and local-charge conservation.
- Darwin model avoids solving fast light speed modes.
- Important numerical performance gain compared to state-of-the-art explicit PIC codes:

$$\frac{CPU_{exp}}{CPU_{imp}} \sim \frac{0.01}{(k\lambda_D)^d}\frac{c}{v_A}\min\left[\frac{1}{k\lambda_D}, \frac{c}{v_A}\sqrt{\frac{m_e}{m_i}}, \sqrt{\frac{m_i}{m_e}}\right]\frac{1}{N_{FE}}$$

- Back-of-the envelope speedup estimate (*a la* Chen 14) with EPT plasma:

  1D -> O(10-100)

  2D -> O(2500)

  3D -> O(60000)

- Wall time in ES case is x30 less than time-explicit Vlasov code [Sánchez et al 2018] for same problem and same or greater accuracy
- New electron push algorithm based on segments offers x5.5 times savings wrt implicit code at LANL
- Wall time scaling:

Increasing need for subcycling for increasing Δt means that there is optimal Δt

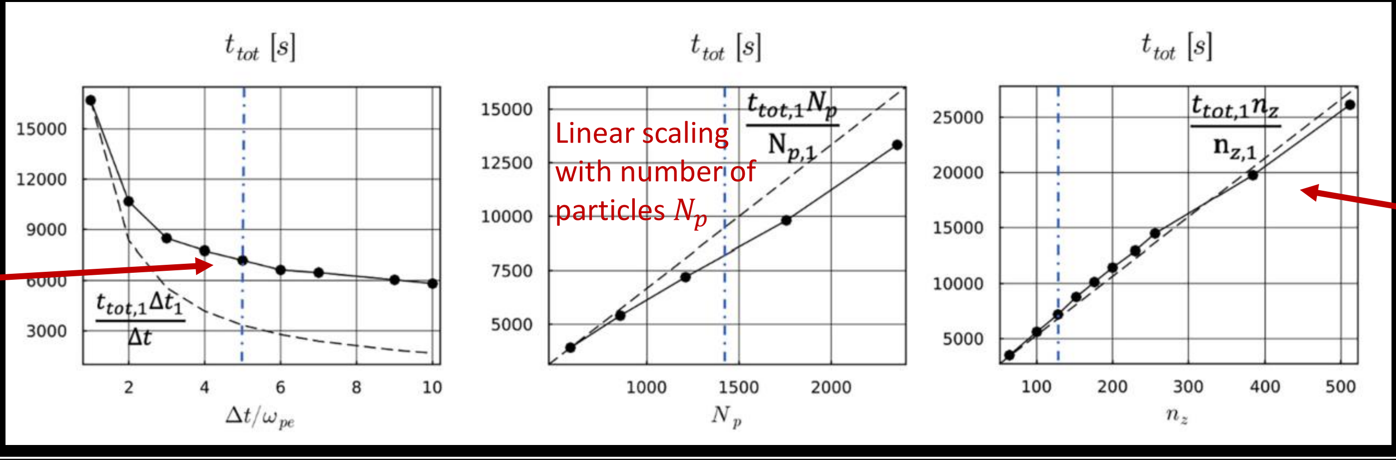

Linear t_{tot} on n_z (number of cells); previous codes at LANL were quadratic on n_z

Magnetic Arch plasma expansion

- A Magnetic Arch (MA) forms when two MNs of opposing polarities are placed next to each other
  - Interesting for clustering MN-EPTs in pairs
  - The magnetic moment of each MN cancels out (beneficial for S/C ADCS)
  - Enables differential thrust vectoring
  - MA can be designed to feature a lower divergence angle than MNs (lower impact of plume on S/C)
- Plasma expansion is now fully 3D and quite distinct from that in a MN. Interesting aspects:
  - Interaction of the two "beamlets" in the central part of the arch
  - Role of the plasma-induced magnetic field likely different from that in a MN

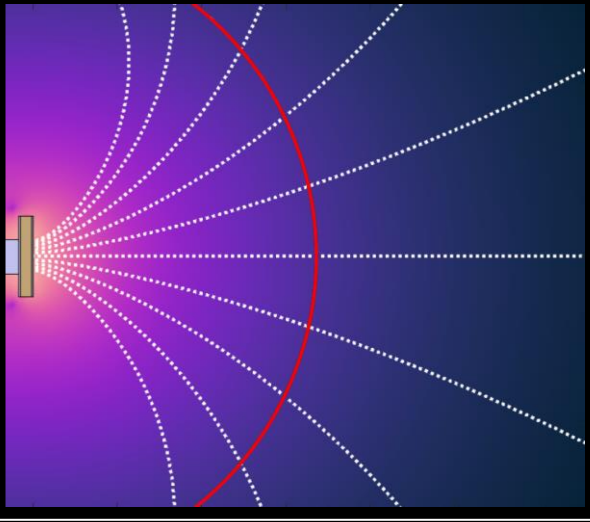

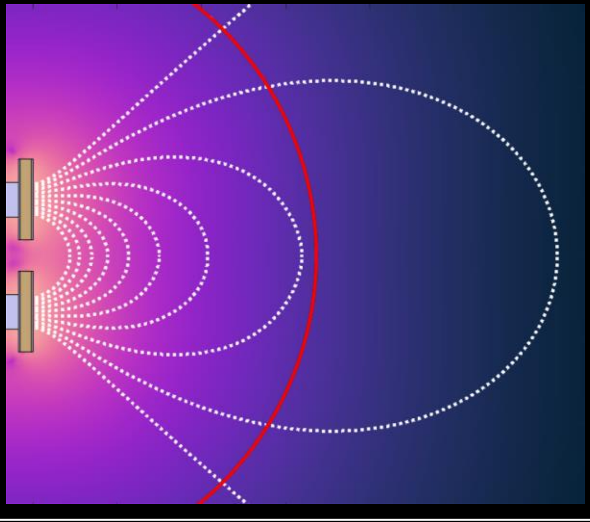

MA (C. Boyé)

MAGNETIC ARCH - DGFEM

- **Two-fluid model in planar approximation**
  - Time dependent. quasineutral,
  - collisionless plasma χ (Hall parameter) $= \infty$
  - Cold, singly-charged ions
  - Massless, polytropic ($\gamma = 1.2$) magnetized electrons:
    - Electron momentum equation is algebraic
    - Thermalized potential Φ and out-of-plane velocity u_{ye} are constant along $\boldsymbol{B}$ lines and fully determined by inlet BCs.
- Discontinuous Galerkin spacial discretization (weak form, Local Lax-Friedrich fluxes).
- Strong stability preserving Runge-Kutta time stepping.

- Gaussian density profile.
  - Radius $R_p = 1$
- Supersonic inlet velocity.
- Supersonic outlet boundary conditions.
- Symmetry plane between the two sources

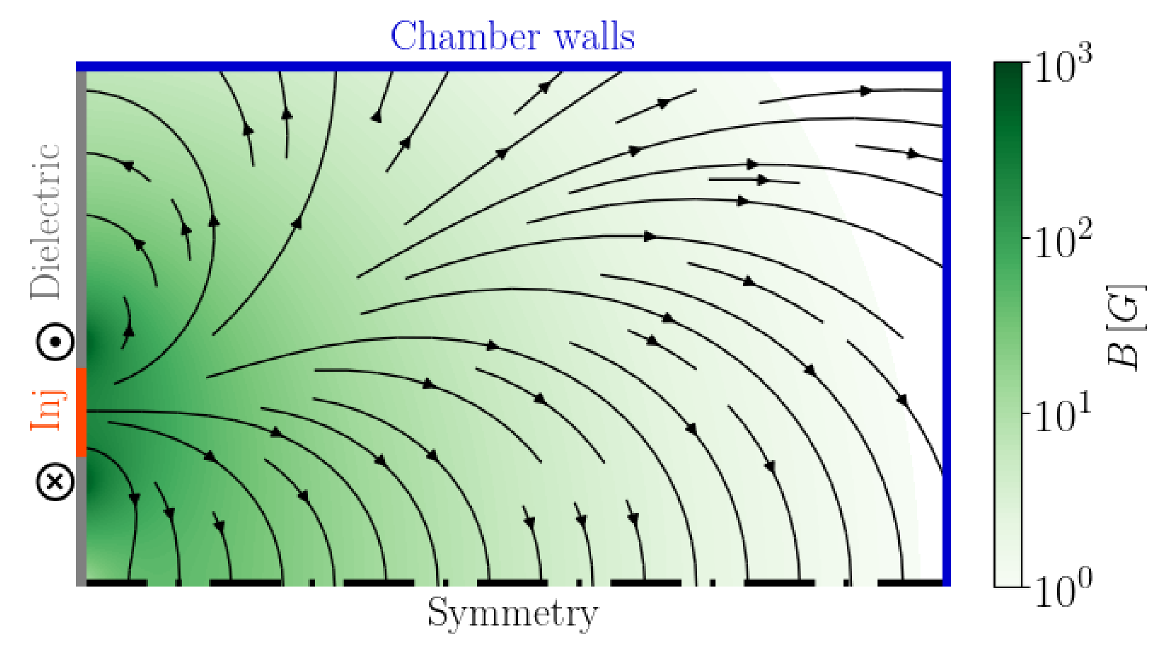

Magnetic Arch – DGFEM

- Initial expansion is similar to standard MNs.
- Oblique shock forms near the symmetry plane, at the beamlet interaction region
- Ions are unmagnetized and expand across the closed field lines.

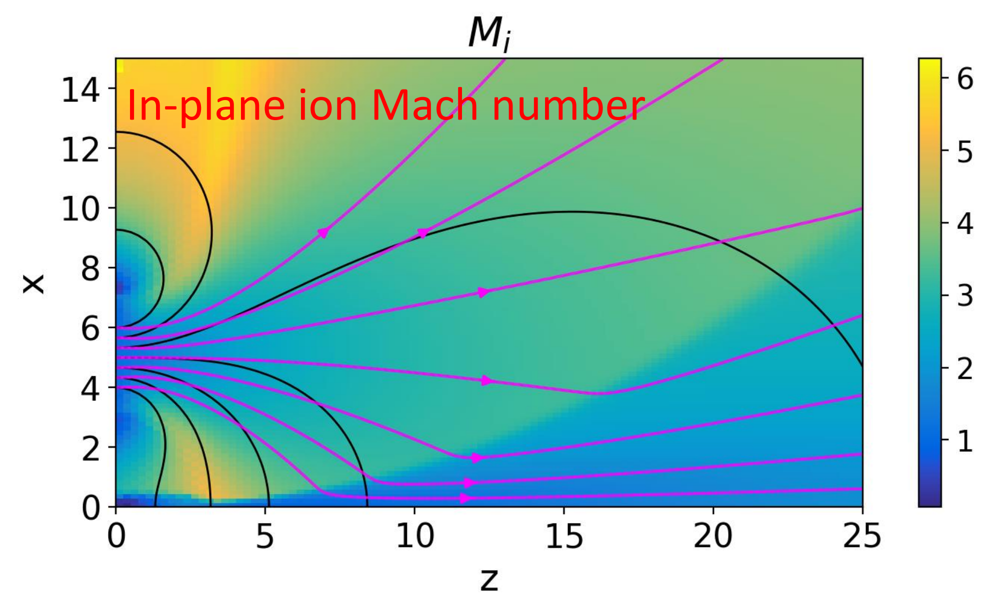

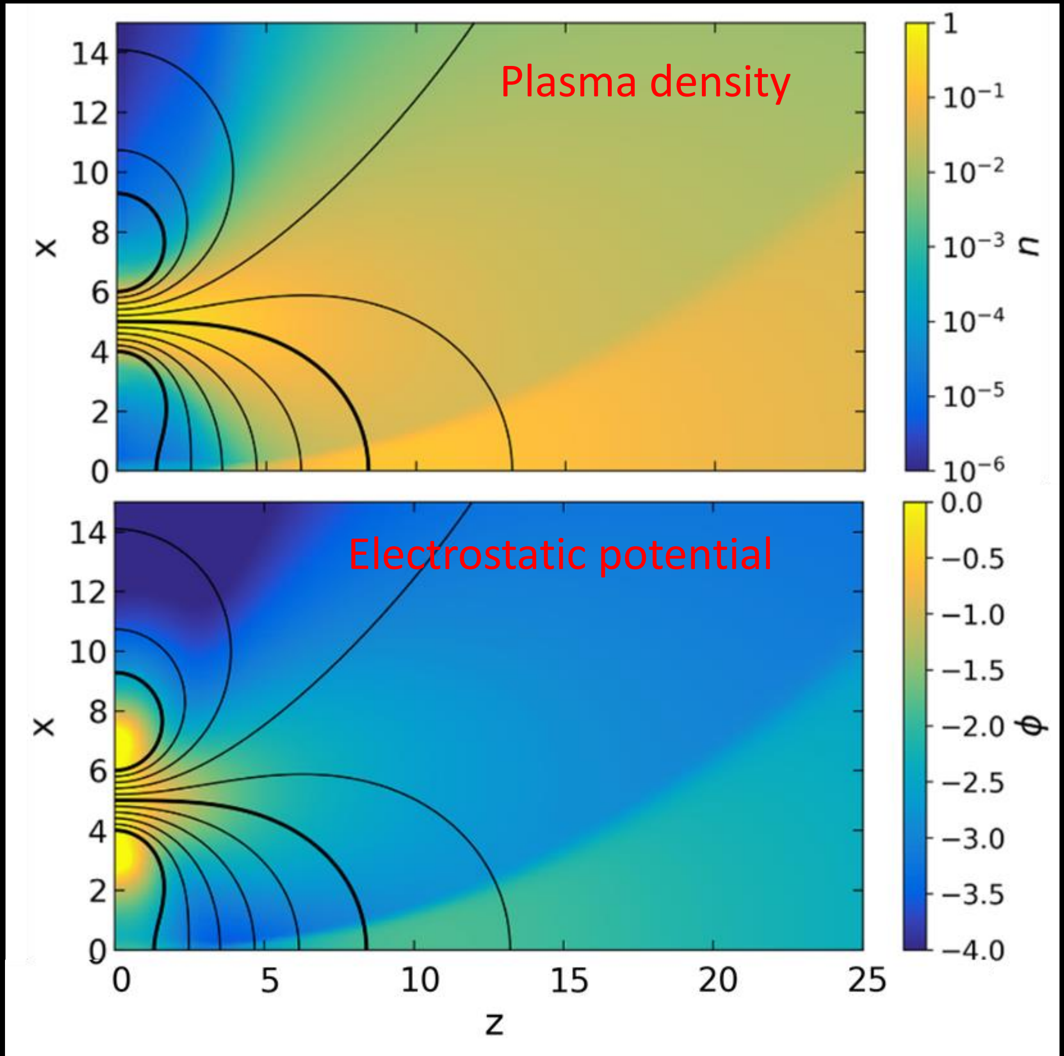

Magnetic Arch – DGFEM

- Magnetic thrust originates from the reaction to the magnetic force density $f_z = enu_{ye}B_x$
  - Ions being essentially unmagnetized ($u_{yi} \simeq 0$) do not contribute to the magnetic force
- A deceleration region appears in regions where $f_z < 0$,

due to the electric potential rise

- Differential thrust force $F(z)$ increases up to a maximum; drag in the downstream region makes it decrease

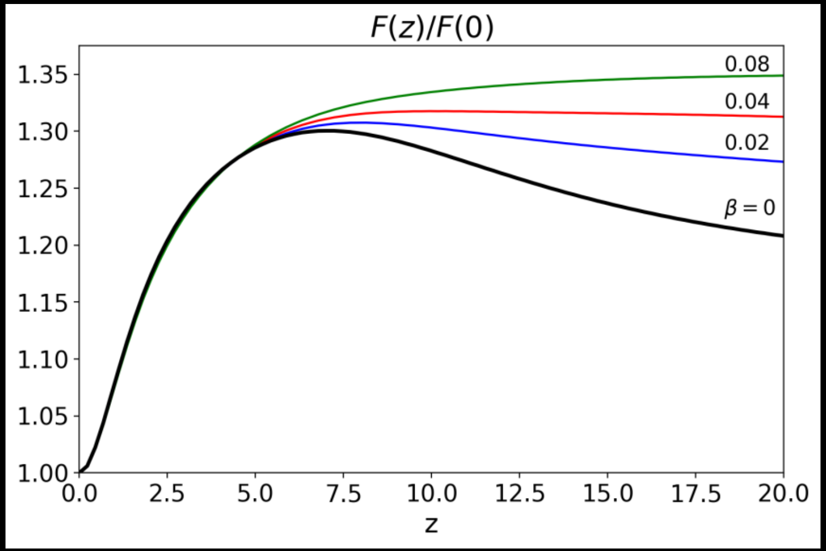

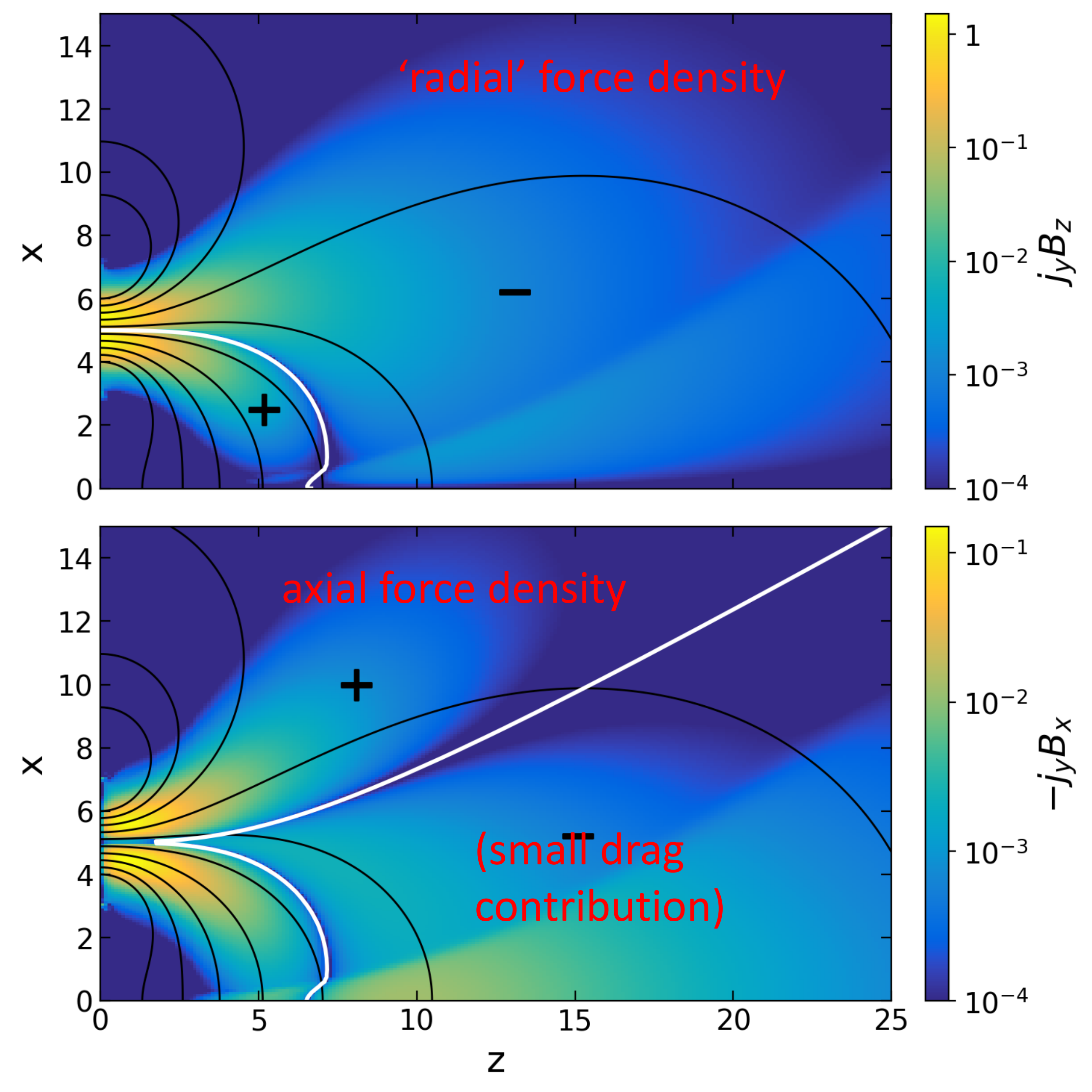

Magnetic Arch – DGFEM

- Incremental thrust force increases up to a maximum; drag in the downstream region makes it decrease
- Effect of the self-induced B-field ($\beta \neq 0$):
  - Diamagnetic electron current tends to “open” the B-lines.
  - Downstream drag force is reduced

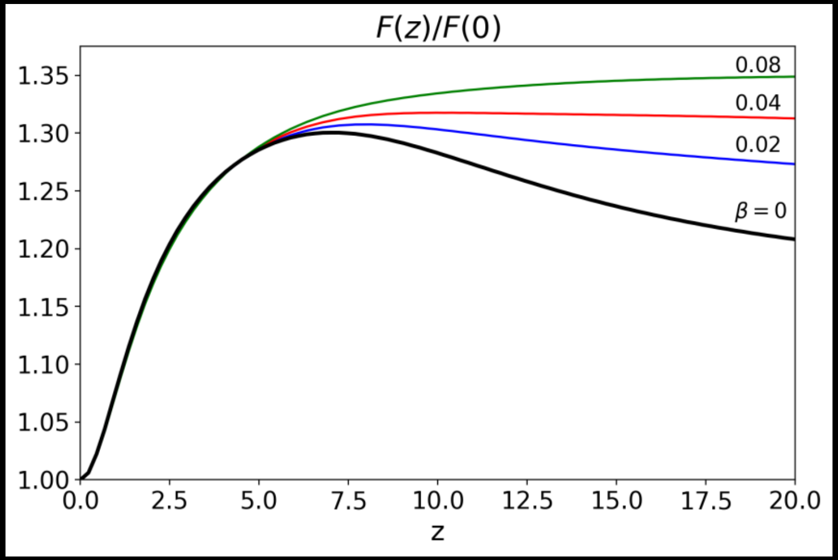

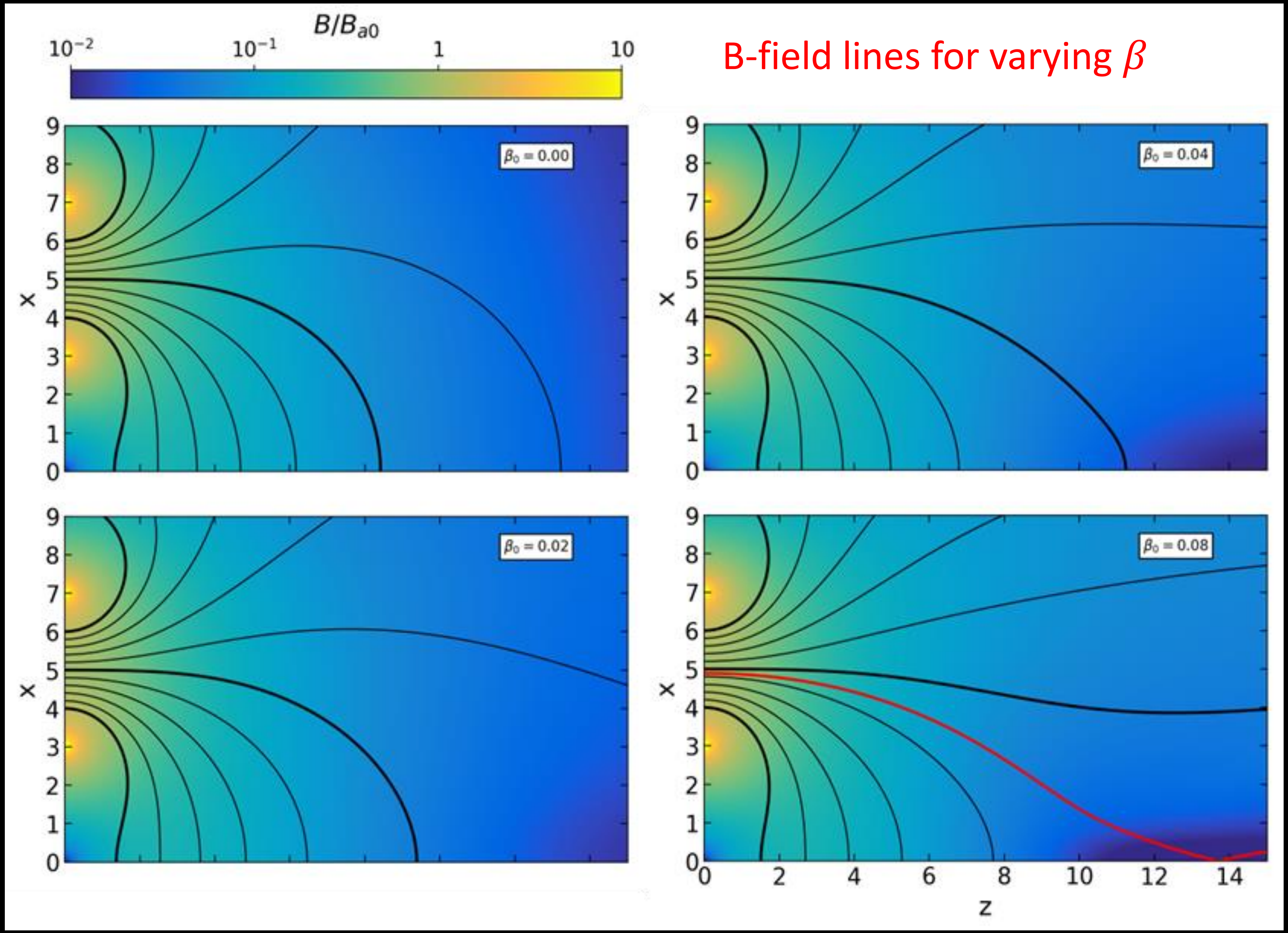

MAGNETIC ARCH – HYBRID CODE

- Same problem, more detailed model.
- **EP2PLUS** code (used successfully in 3D plume simulation) is used in 2D planar mode. Composed of a
  - Heavy species Module (ions and neutrals): PIC formulation
  - Electron module: Drift-diffusion, magnetized fluid model
- Improvements wrt to previous fluidmodel:
  - Access to multibeam ion VDF
  - Effects of collisionality on electrons (ionization, elastic,…)
    → χ (Hall parameter) is finite
    → Mathematically different from case $\chi = \infty$
  - Effects of background pressure
  - Effects of the external boundary conditions

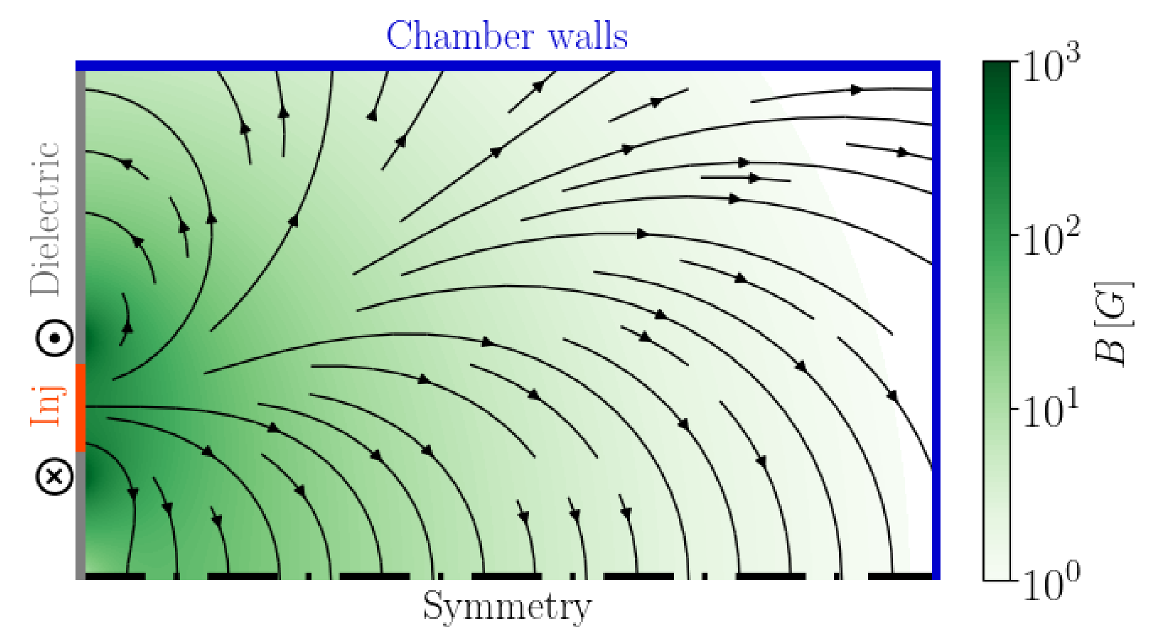

MAGNETIC ARCH – HYBRID CODE

- Symmetric and 2D planar simulation domain, identical to the two-fluid study
- $\beta = 0$ in all cases studied (no induced $\boldsymbol{B}$ field)
- Plasma composed of:
  - Singly charged Xenon ions
  - Electrons
  - Simplified neutral background and collisionality:

$$\chi = 30,\ \sigma_e = en\chi/B,\ \mathbf{j}_c = 0$$

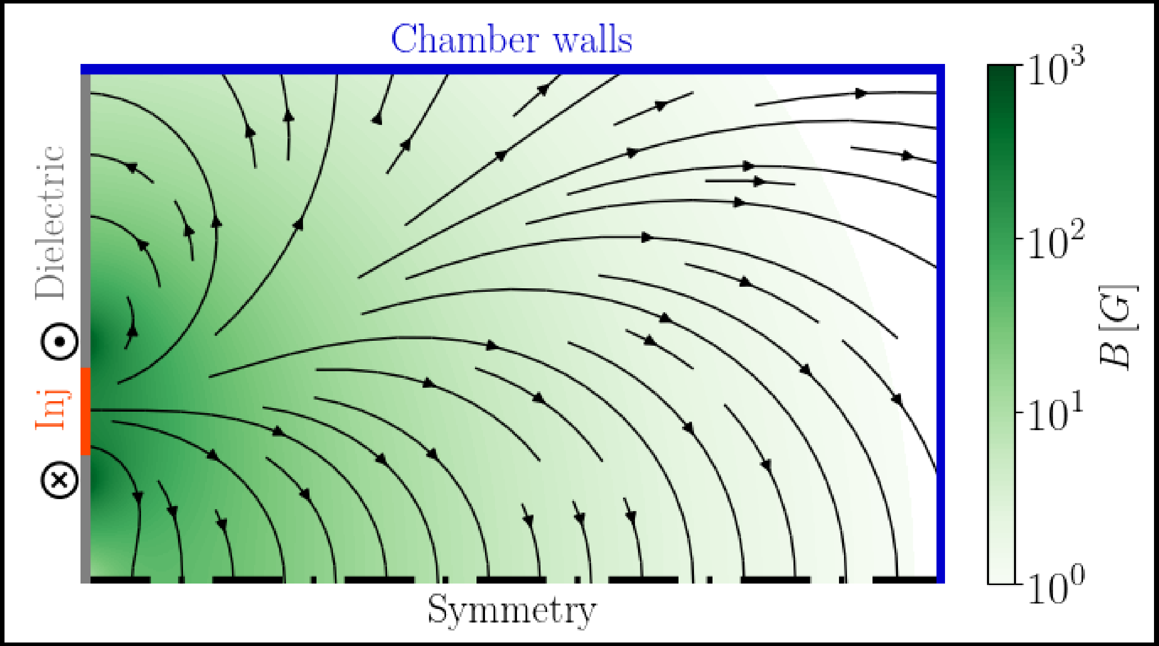

- Boundary Conditions:
  - Injection:
    - Gaussian density profile, sonic ions
    - Uniform electric potential: $\phi = 0$
  - Symmetry:
    - Reflect all particles
    - Null electron current
  - Dielectric:
    - Absorb all particles
    - Impose $j_{en} = -j_{in}$
  - Chamber walls:
    - Absorb all particles
    - Impose $I_{eW} = -I_{iW}$

Parameter	Value
n_0	$10^{18}\ m^{-3}$
T_{e0}	$5\ eV$
γ	1.2

Magnetic Arch – Hybrid code – Plasma Response

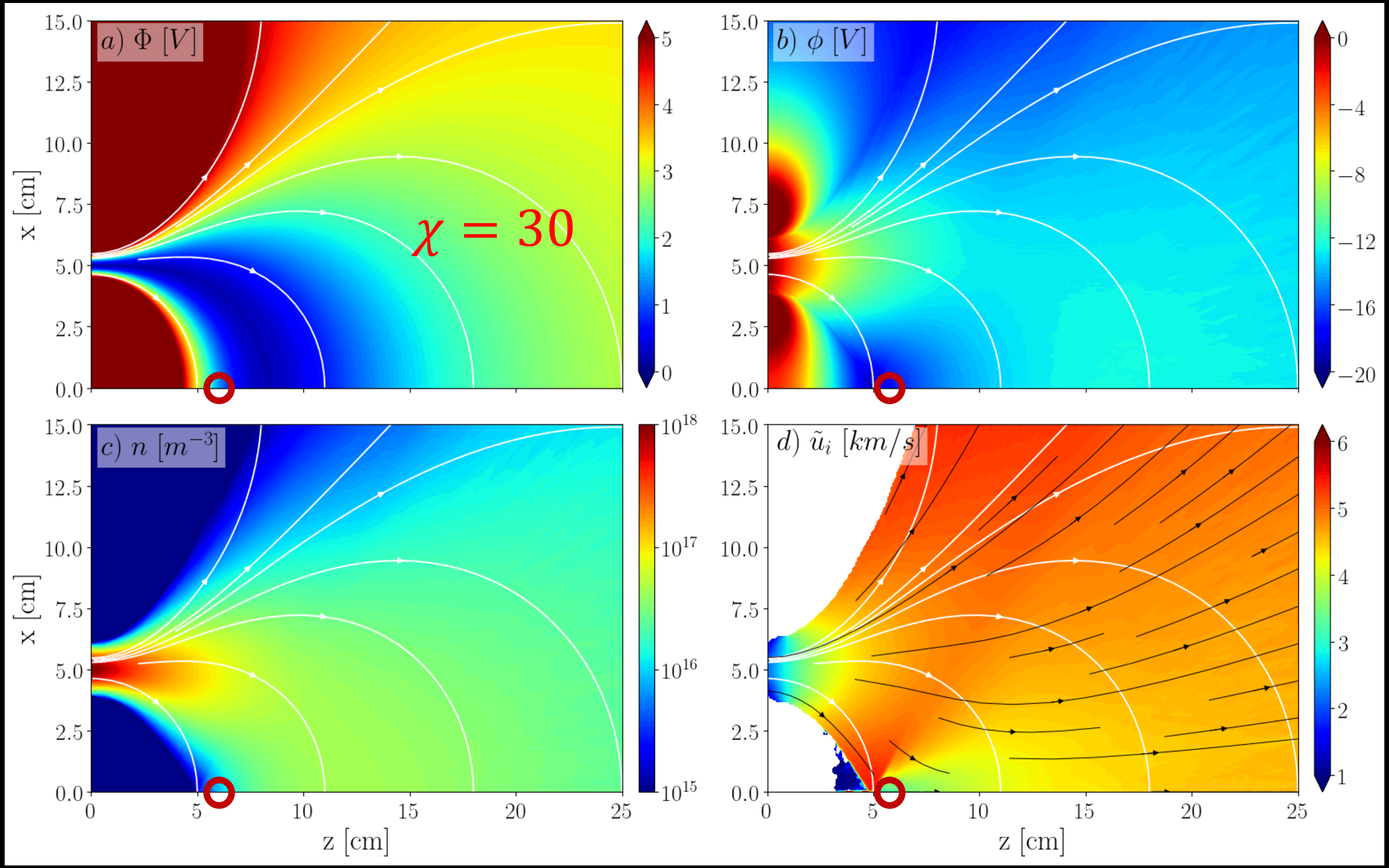

- Thermalized potential is ~constant along magnetic lines
- No clean shock structure is present (although n and ϕ do rise in the interaction region, and $\tilde{u}_i$ does feature a sharp change)
- PIC algorithm enables access to IVDF: at the interaction region results from the combination of two ion populations

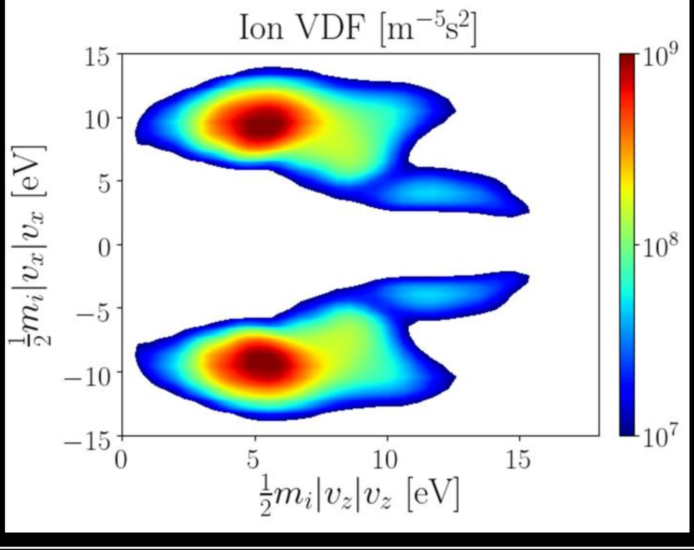

MAGNETIC ARCH – HYBRID CODE – EFFECTS OF MAGNETIZATION

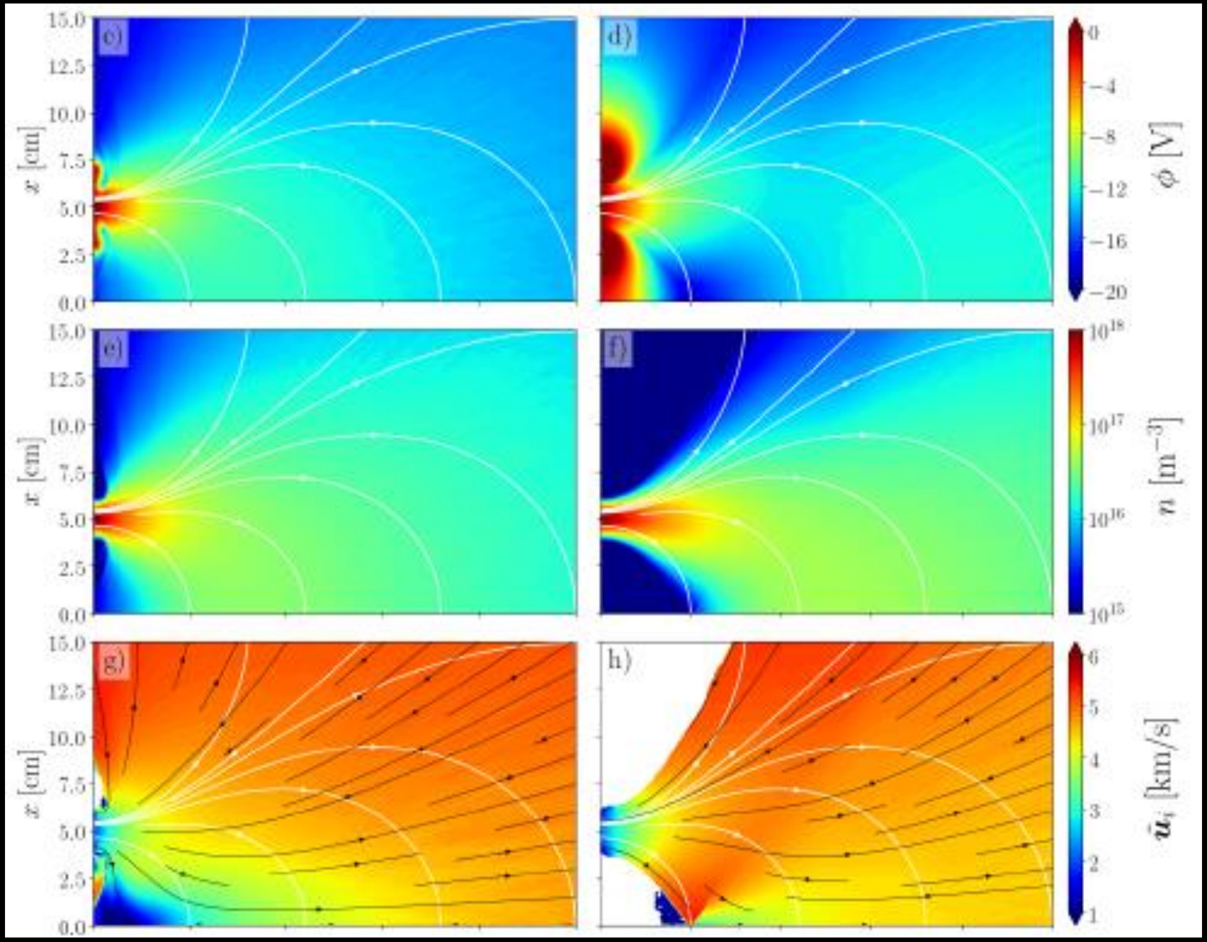

- Comparison of $\chi = 3$ and $\chi \geq 10$. (with $B_0 \propto \chi$)
  - Simulations with $\chi \geq 10$ showed very similar results, except for in-plane electron currents
  - At $\chi = 3$,the MN effects starts to fade
    - Little magnetic guiding
    - Little magnetic thrust

A case with background pressure. Ionization in the plume increases the flow of ions and hence thrust

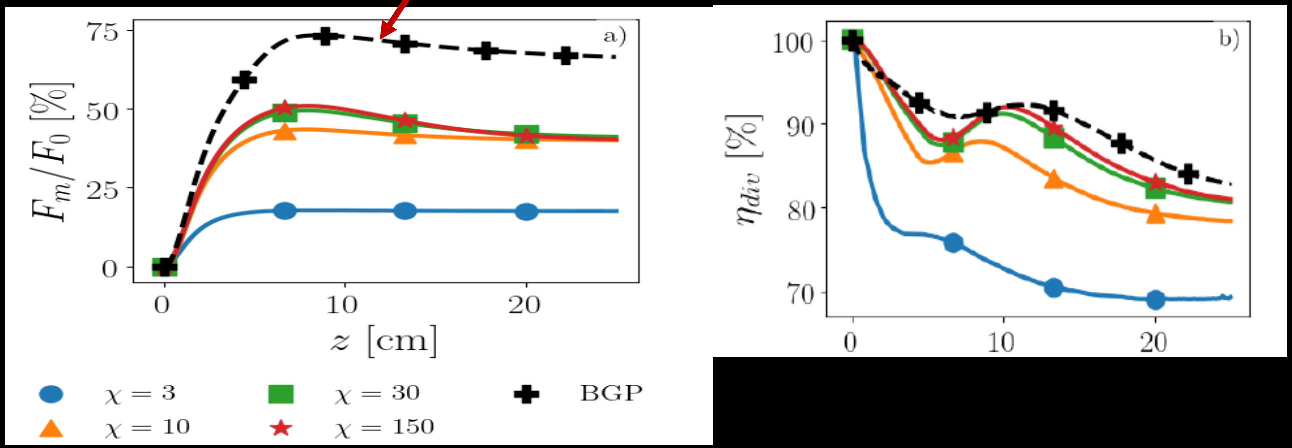

MAGNETIC ARCH – HYBRID CODE – BOUNDARY CONDITIONS

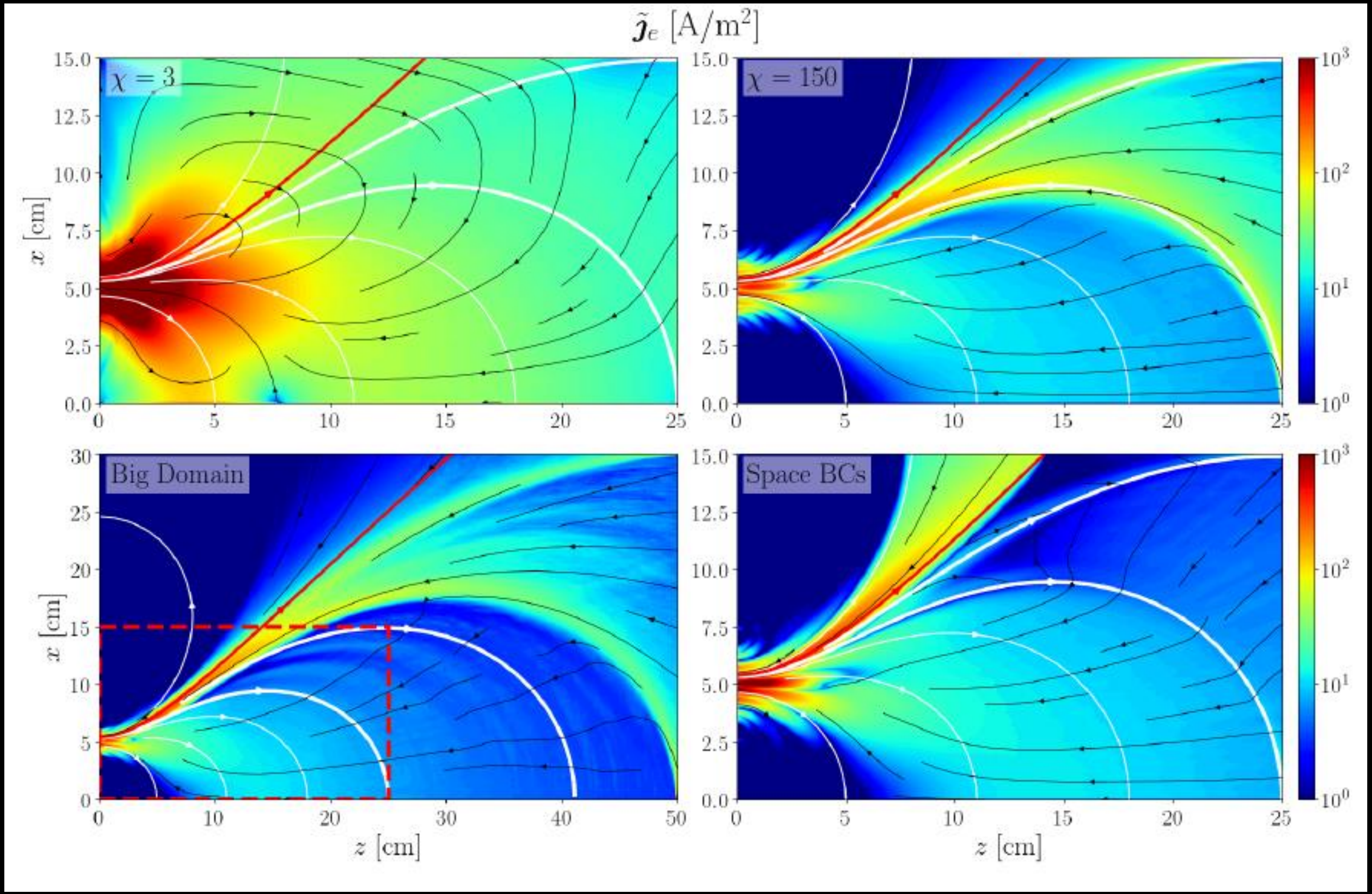

- In-plane electron currents are very sensitive to Hall parameter and to conditions in the external boundaries.
- Last point is a serious issue when a finite numerical domain wants to represent the expansion in free-space or on a very large chamber.
- The 3 simulations for $\chi = 150$ are a good example.
- Fortunately, in-plane electron currents are almost decoupled from the rest of plasma variables

SUMMARY

- Time-implicit, energy- and charge-conserving PIC codes + Darwin model offer a complete yet fast scheme for low-temperature, magnetized plasma simulations, relevant for electric propulsion
  - Overcomes λ_{De} and ω_{pe} scaling of grid and timestep to tackle larger problems faster
- Q1D3V Magnetic Nozzle with a RHP wave shows that waves from the source may propagate and be absorbed in the plume, affecting the kinetic response of electrons and hence the plasma expansion
  - x30 time saving wrt same problem solved with explicit Vlasov. Greater savings expected in higher dimensions
  - A simple cold-plasma wave model can be tuned using the EM-kinetic MN simulation to yield accurate results: there is value in simpler models, augmented with fit laws for certain parameters
- Magnetic Arch simulation (two MNs with opposing polarities) shows that a plasma jet can be extracted from the closed-line configuration, generating magnetic thrust
  - The plasma-induced magnetic field plays a central role in the MA, more so than in a MN
  - Collisions affect negatively the performance, but effective Hall parameter of $\chi \sim 10$ suffice to observe the MN/MA effect
  - The comparison of fluid and hybrid models in the same Magnetic Arch case affords a valuable comparative study
- Multi-tiered simulation approach to plasma thrusters and plumes is likely the best approach to combine accuracy (complex, kinetic-electromagnetic codes) and speed (simple, tuned fluid and wave codes).
  We find this is the way forward toward a versatile, predictive simulation facility

ACKNOWLEDGMENTS

This project has received funding from the European Research Council (ERC) under the European Union's Horizon 2020 research and innovation programme (grant agreement No 950466)

European Research Council
Established by the European Commission

THANK YOU!

mario.merino@uc3m.es,

ZARATHUSTRA

EP² uc3m erc

Magnetic Arch – Hybrid code

- Same problem, different model: access to IEDF, effects of collisionality / incomplete electron magnetization
- EP2PLUS code (used successfully in 3D plume simulation) is used in 2D planar mode
- Composed of a **Heavy Species Module** (ions and neutrals) and a **Fluid Module** (electrons).

Heavy Species Module

- Ion and neutral macroparticles
- Standard PIC-MC algorithms
- Momentum conserving

Fluid Module

- Quasi-neutral plasma
- Electrons are quasi-stationary and inertialess, with an isotropic, diagonal temperature tensor
- We solve the **continuity** and **momentum equations**, closed with a **polytropic law**

$$\nabla \cdot \mathbf{j} = 0$$

$$\mathbf{j} = -\mathcal{K} \cdot (\sigma_e \nabla \Phi + \mathbf{j}_c) + \mathbf{j}_i$$

with:

$$\Phi = \phi + \frac{\gamma}{e(\gamma - 1)} T_{e0} \left[1 - \left(\frac{n}{n_0} \right)^{\gamma - 1} \right], \qquad \mathcal{K} = \frac{1}{1+\chi^2} \begin{bmatrix} 1+\chi^2 & 0 & 0 \\ 0 & 1 & -\chi \\ 0 & \chi & 1 \end{bmatrix}$$

$$\sigma_e = e^2 n / (m_e \nu_e), \qquad \mathbf{j}_c = (en/\nu_e) \sum_s \nu_{es} \mathbf{u}_s$$